Eur. Phys. J. C 6, 297–306 (1999)
DOI 10.1007/s100529800912

THE EUROPEAN PHYSICAL JOURNAL C

Two–loop integrals in chiral perturbation theory

J. Gasser[1], M.E. Sainio[2]

[1] Institute of Theoretical Physics, University of Berne, Sidlerstrasse 5, CH–3012 Berne, Switzerland
[2] Department of Physics, University of Helsinki, P.O. Box 9, FIN–00014 Helsinki, Finland

Received: 14 April 1998 / Published online: 7 August 1998

Abstract. We consider chiral perturbation theory in the meson sector at order E^6. In the terminology of the external field technique, the genuine two–loop diagrams so generated are of the sunset type. We discuss the evaluation of several of these in the case where the masses of the particles running in the loops are equal. In particular, we present integral representations that are suitable for the evaluation of diagrams in kinematical regions where branch points and cuts are present.

1 Introduction

In the framework of chiral perturbation theory (CHPT) [1], Green functions are expanded in powers of the external momenta and of the light quark masses. The generating functional is constructed by use of an effective lagrangian and requires the evaluation of tree graphs at leading order, one–loop graphs at next–to–leading order, and two–loop graphs at next–to–next–to–leading order. In this article, we describe the evaluation of several two–loop graphs in the equal mass case.

The first complete two–loop calculation in CHPT was performed in [2], in order to investigate the apparent discrepancy of the one–loop prediction [3] of the cross section $\gamma\gamma \to \pi^0\pi^0$ with the data [4]. The topologies of the two–loop graphs considered in [2] contain the ones in

$$\begin{aligned} &- \text{ vector and axialvector two–point functions} \\ &- \pi \to e\nu\gamma \\ &- \text{ scalar and vector form factors of the pion} \\ &- \pi\pi \to \pi\pi \\ &- \gamma\gamma \to \pi^+\pi^- \end{aligned} \qquad (1)$$

In other words, knowing how to evaluate the two–loop graphs in $\gamma\gamma \to \pi^0\pi^0$ allows one to calculate those that occur in (1) in the equal mass case. There are other Green functions where the two–loop graphs have the same topology as (1), e.g. $\pi\pi \to 4\pi$ or $\gamma \to 4\pi$. The external momenta in those processes are, however, in a different kinematical region than in (1), and the integral representations worked out below do not apply.

The evaluation of the two–loop integrals in (1) is not straightforward for several reasons: i) CHPT being a low–energy expansion, one has to keep all masses at their physical values – the zero mass limit would result in a poor approximation of the matrix element. ii) The interaction is of the derivative type, which generates polynomials of high degree in the numerator of the loop–integrals. iii) In general, one needs the loop–functions in a region where branch points and cuts are present.

Since the work of [2], additional two–loop calculations have been performed. In the two flavour sector, these are the amplitudes for $\gamma\gamma \to \pi^+\pi^-$ [5], $\pi \to e\nu\gamma$ [6] and $\pi\pi \to \pi\pi$ [7]. In the three flavour sector, there exist calculations of the vector [8] and axialvector [9] two–point functions, and of a combination of vector form factors [10]. For a review of these calculations, we refer the reader to [11].

The calculational methods developed in [2] were applied in [5–7,9,12]. As these techniques were never made public in a coherent manner, we wish to do so here. At the same time, we use the opportunity to simplify the originally used calculational tools.

We are, of course, aware that this is not the first publication on two–loop integrals. Nevertheless, we feel that it would be inappropriate to give an overview of what has been previously done in this field, because those calculations are, as far as we can judge, mostly unrelated to what we aim at here. Indeed, in contrast to e.g. the evaluation of two–loop integrals in the framework of the Standard Model, where very different mass scales occur, the present article deals with applications in $SU(2) \times SU(2)$ CHPT, where the masses are equal. Furthermore, there is only a limited number of two–loop graphs that will ever need to be calculated. We expect that the techniques presented below will be useful in this restricted framework, because they represent a coherent method to deal with quite different topologies. In addition, the same methods can also be applied in chiral $SU(3) \times SU(3)$ – where the masses are different – see [9] for the self–energy graph. To give another illustration, we expect that the two–loop graphs in K_{l4} decays at order E^6 can be worked out with these methods in a straightforward (yet admittedly tedious) manner.

The article is organized as follows. In Sect. 2, we elucidate the structure of the terms at order E^6 in the chiral expansion, in particular the role of the two–loop diagrams. The following sections are devoted to the evaluation of the

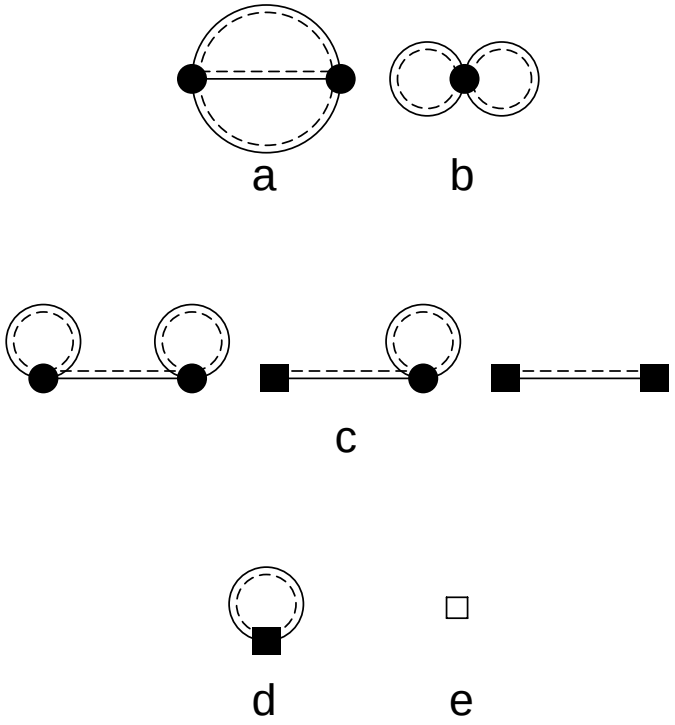

Fig. 1a–e. Contributions to the generating functional at order E^6. The solid–dash lines denote the propagator in the presence of the external fields. Filled circles (filled squares) denote vertices from the effective lagrangians $\mathcal{L}_2$ ($\mathcal{L}_4$) in (2). The open square in **e** stands for vertices from $\mathcal{L}_6$. Only the sunset diagram **a** generates genuine two–loop integrals

self–energy (Sect. 3), the vertex (Sect. 4), the box (Sect. 5) and the acnode diagram (Sect. 6). Section 7 contains the summary and concluding remarks. The notation is given in appendix A, whereas appendix B contains one–loop integrals. The divergences are evaluated and tabulated in appendix C.

2 The diagrams at order E^6

The effective lagrangian of QCD in the meson sector consists of a string of terms,

$$\mathcal{L}_{\mathit{eff}} = \mathcal{L}_2 + \hbar\mathcal{L}_4 + \hbar^2\mathcal{L}_6 + \cdots , \qquad (2)$$

where tree graphs with $\mathcal{L}_N$ generate polynomial contributions of order E^N in the energy expansion. These lagrangians contain external sources which allow one to evaluate the transition amplitudes with the background field method. The path integral representation of the generating functional is

$$e^{iZ/\hbar} = \int [dU] e^{i/\hbar \int dx\, \mathcal{L}_{\mathit{eff}}} ,$$

where $[dU]$ denotes the chiral invariant measure. The low–energy representation

$$Z = Z_2 + \hbar Z_4 + \hbar^2 Z_6 + \cdots$$

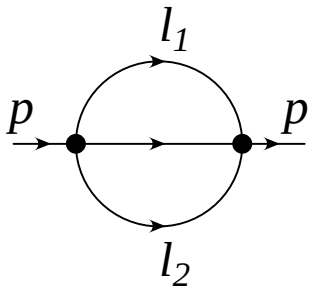

Fig. 2. The self–energy diagram. The filled circles denote vertices from the effective lagrangian $\mathcal{L}_2$ in (2). The internal lines stand for scalar propagators with mass 1

is obtained by expanding the lagrangians $\mathcal{L}_I$ around the solution of the classical equation of motion $\delta\int dx\, \mathcal{L}_2 = 0$ and carrying out the path integral to the required order in $\hbar$. The diagrams which generate the terms of order E^6 are collected in Z_6 and displayed in Fig. 1. The solid–dash lines stand for the propagator in the presence of the external fields. Full circles (full squares) denote vertices from $\mathcal{L}_2$ ($\mathcal{L}_4$), whereas the open square stands for a vertex from $\mathcal{L}_6$. The diagrams at order E^6 for a specific process are obtained by attaching the external lines in all possible ways to these graphs. Examples are the self–energy, the vertex, the box and the acnode diagram considered below (Figs. 2, 3, 4 and 5, respectively).

Figure 1a collects all genuine two–loop diagrams. It is seen that, in the language of the external field technique, these are of the sunset type. The Figs. 1b–e display diagrams that amount to products of two one–loop integrals, to products of a one–loop integral with a tree graph contribution from $\mathcal{L}_4$, to one–loop graphs with $\mathcal{L}_4$, or to tree graphs alone. In the following, we reserve the term "two–loop integral" to contributions from the sunset graph Fig. 1a. [There are Green functions with no sunset contributions at order E^6 – e.g., the vector two–point functions [8]. The evaluation of these matrix elements then simplifies accordingly.]

In the following, we outline the evaluation of the two–loop diagrams that occur in the process $\gamma\gamma \to \pi^0\pi^0$ in the two flavour case, with equal mass for the particles running in the loops.

3 The self–energy

We evaluate contributions from the self–energy diagram that is displayed in Fig. 2. The case where the masses of the particles running in the loops are not identical is discussed e.g. in [13] with a technique that is very different from the one proposed in this work. References to earlier work on the sunset graph may be found in [13], see also [14].

We consider the integrals[1]

$$(H; H^\mu; H^{\mu\nu}) = \left\langle\left\langle\, (\,1; l_1^\mu; l_1^\mu l_1^\nu\,) \prod_{i=1}^{3} \frac{1}{D_i} \right\rangle\right\rangle , \qquad (3)$$

with

$$D_1 = 1 - l_1^2\,,\ D_2 = 1 - l_2^2\,,\ D_3 = 1 - (p - l_1 - l_2)^2\,. \quad (4)$$

Integration over l_2 generates the loop–function

$$J(t) = C(w)\Gamma(-w) \int_0^1 dx\, [1 - tx(1-x)]^w\,,$$
$$t = (p - l_1)^2\,. \qquad (5)$$

The function $J(t)$ is analytic in the complex $t-$plane, cut along the positive real axis for $t \geq 4$. We insert the Cauchy representation [15]

$$J(t) = \int_4^\infty \frac{[d\sigma]}{\sigma - t}\ \ ;\ \ -1.5 < w < 0\,, \qquad (6)$$

and integrate over l_1. In this manner, we obtain by use of the formulae in appendix B

$$(H; H^\mu) = \int_4^\infty [d\sigma]\, \{F_2[z_2]\ ;\ (1-x)F_2[z_2]\ p^\mu\}_1\ ,$$
$$H^{\mu\nu} = \frac{1}{2}\int_4^\infty [d\sigma]\, \big\{2(1-x)^2 F_2[z_2]\ p^\mu p^\nu - F_1[z_2]\ g^{\mu\nu}\big\}_1\ ,$$
$$z_2 = (1 - s(1-x))\, x + \sigma(1-x)\ ;\ s = p^2\,. \qquad (7)$$

The integration over the variable σ in (7) converges in the strip

$$-1.5 < \mathrm{Re}\ w < -1\,.$$

Using partial integration in x for the last term in $H^{\mu\nu}$, the nontrivial integrals in (7) reduce to

$$\int_4^\infty [d\sigma]\, \{(1-x)^m F_2[z_2]\}_1\ . \qquad (8)$$

It remains to extract the finite and infinite parts in (8) as $w \to 0$. We subtract and add the first two terms of the Taylor series of $F_2[z_2]$ around $s = 1$. The finite part becomes

$$\int_4^\infty d\sigma\beta\, \{(1-x)^m \mathcal{K}_2(x,\sigma;s)\}_1\ , \qquad (9)$$

where we have introduced the kernel

$$\mathcal{K}_2(x,\sigma;s) = -\frac{1}{(16\pi^2)^2} \times \left\{\ln\frac{z_2}{z_2^{s=1}} + (s-1)\frac{x(1-x)}{z_2^{s=1}}\right\}\,. \quad (10)$$

It vanishes at $s = 1$, together with its first derivative,

$$\mathcal{K}_2(x,\sigma;1) = \mathcal{K}_2'(x,\sigma;1) = 0\,,$$

and dies off rapidly at large values for σ,

$$\mathcal{K}_2 = O\left(\frac{1}{\sigma^2}\right)\,,\ \sigma \to \infty\,.$$

The infinite part of (8) may be expressed in terms of the quantities

$$D(m,n) = \int_4^\infty [d\sigma]\, \{(1-x)^m F_n[y]\}_1\ ,$$
$$y = x^2 + \sigma(1-x)\,, \qquad (11)$$

that are evaluated and tabulated in appendix C. As an illustration of the method, we consider the scalar integral $H(s)$. The subtracted function

$$\underline{\underline{H}}(s) = H(s) - H(1) - (s-1)H'(1)$$

stays finite as $w \to 0$,

$$\underline{\underline{H}}(s) = \int_4^\infty d\sigma\beta\, \{\mathcal{K}_2(x,\sigma;s)\}_1\ . \qquad (12)$$

The poles at $w = 0$ are contained in $H(1)$ and in $H'(1)$,

$$H(1) = D(0,2) = -C^2(w)\Gamma^2(-w)\left\{\frac{3}{2} - \frac{17}{4}w + \frac{59}{8}w^2 + O(w^3)\right\}\,,$$
$$H'(1) = 2\,\{D(1,3) - D(2,3)\} = -C^2(w)\Gamma^2(-w)\left\{\frac{1}{4}w + \frac{3}{8}w^2 + O(w^3)\right\}\,. \qquad (13)$$

The representation (12) is well suited for numerical evaluation at $s < 9$ only. In the region $s > 9$, $H(s)$ develops an imaginary part. At $d = 4$,

$$\mathrm{Im}H(s) = \frac{\pi}{s(16\pi^2)^2}\int_4^{(\sqrt{s}-1)^2} d\sigma\beta[s - (\sqrt{\sigma}+1)^2]^{1/2} \times [s - (\sqrt{\sigma}-1)^2]^{1/2}\,. \qquad (14)$$

As a result, one has the dispersion relation

$$\underline{\underline{H}}(s) = \frac{(s-1)^2}{\pi}\int_9^\infty \frac{dz\,\mathrm{Im}H(z)}{(z-1)^2(z-s)}\,, \qquad (15)$$

that allows one to evaluate $\underline{\underline{H}}$ also at $s > 9$. A similar remark applies to the Lorentz invariant components of the tensorial integrals H^μ and $H^{\mu\nu}$.

4 The vertex

4.1 Tensorial integrals

Here we consider the vertex diagram Fig. 3 that leads to the integrals

$$\left\langle\left\langle\, (\,1\,;\, l_1^\mu\,;\, l_1^\mu l_1^\nu\,) \prod_{i=1}^{4} \frac{1}{D_i} \right\rangle\right\rangle\,, \qquad (16)$$

[1] The notation is given in appendix A

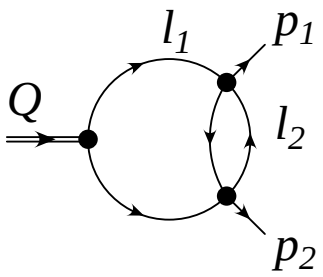

Fig. 3. The vertex diagram. The filled circles denote vertices from the effective lagrangian $\mathcal{L}_2$ in (2). The double external line denotes a current of momentum Q, e.g. one scalar or two electromagnetic currents (contact term). The internal lines stand for scalar propagators with mass 1

with

$$\begin{aligned} &D_1 = 1 - l_1^2\,,\ D_2 = 1 - (Q - l_1)^2\,,\\ &D_3 = 1 - l_2^2\,,\ D_4 = 1 - (l_2 + l_1 - p_1)^2\,,\\ &Q = p_1 + p_2\,,\ p_1^2 = p_2^2 = 1\,. \end{aligned} \tag{17}$$

Integration over l_2 gives the loop–function $J(\bar{t})$ with $\bar{t} = (p_1 - l_1)^2$, that we represent in the dispersive manner (6). We subtract the emerging subdivergence by writing $J(\bar{t}) = J(0) + \bar{J}(\bar{t})$. The contribution from $J(0)$ generates a nonlocal divergence that is removed by the usual renormalization procedure. We do not consider this piece any further and concentrate on the remainder,

$$(V\,;V^\mu\,;V^{\mu\nu}) = \int_4^\infty \frac{[d\sigma]}{\sigma} \left\langle \frac{(1\,;l_1^\mu\,;l_1^\mu l_1^\nu)\,\bar{t}}{D_1 D_2(\sigma - \bar{t})} \right\rangle\,. \tag{18}$$

We collect the denominators by $\mathcal{F}[D_1 D_2(\sigma - \bar{t})]$ and rename the Feynman parameters for later convenience,

$$x_1, x_2 \to x_2, x_3\,,$$

such that

$$\begin{aligned} (V\,;V^\mu\,;V^{\mu\nu}) &= \int_4^\infty \frac{[d\sigma]}{\sigma} \left\{ \left\langle \frac{(1;l_1^\mu;l_1^\mu l_1^\nu)\bar{t}}{[z_3 - (l_1 - R)^2]^3} \right\rangle \right\}_{23}\,,\\ z_3 &= \sigma(1 - x_3) + x_3^2 y_2\,,\\ y_2 &= 1 - s x_2(1 - x_2)\,,\\ R &= (1 - x_2)x_3 Q + (1 - x_3)p_1\,,\\ s &= Q^2 = 2p_1 Q = 2p_2 Q\,. \end{aligned} \tag{19}$$

After the shift $l_1 \to l_1 + R$ the momentum integration may be performed with (B1), and the tensors $V^\mu, V^{\mu\nu}$ can be expressed in terms of the scalar integrals

$$V_m[P;s] = \int_4^\infty \frac{[d\sigma]}{\sigma} \left\{P(x_2,x_3) F_m[z_3]\right\}_{23}\,, \tag{20}$$

where $P(x_2, x_3)$ is a polynomial in x_2, x_3, and where the argument s in $V_m[P;s]$ denotes the s–dependence of z_3. This procedure automatically generates the tensorial structure in the external momenta. The integrals (20) can be decomposed into the convergent integral $V_3[P;s]$ and the divergent polynomials $V_1[P;0]$, $V_2[P;0]$ by use of the recursion relation

$$\begin{aligned} V_m[P;s] &= V_m[P_1(1,x_3);0]\\ &\quad + m V_{m+1}[s[x_3^2(2x_2 - 1)]P_1;s]\,,\\ P_1(x_2,x_3) &= \int_0^{x_2} P(y,x_3)dy\,, \end{aligned} \tag{21}$$

obtained from (20) by partial integration in x_2. Finally, $V_1[P;0]$ and $V_2[P;0]$ may be expressed in terms of the integrals

$$\begin{aligned} E(m,n) &= \int_4^\infty \frac{[d\sigma]}{\sigma} \left\{(1-x)^m F_n[y]\right\}_1\,,\\ y &= x^2 + \sigma(1 - x)\,, \end{aligned} \tag{22}$$

that are evaluated and tabulated in appendix C. In the following subsection we illustrate the procedure in case of the scalar integral $V(s)$.

4.2 The scalar integral

Performing the above described procedure, the scalar integral $V(s)$ becomes

$$\begin{aligned} V(s) &= V_3[P_s;s] - (w+2)\left\{E(0,2) - E(1,2)\right\}\,,\\ P_s &= x_3^2\{y_2 + s(w+2)(1 - 2x_2)x_2\}\,. \end{aligned} \tag{23}$$

As $w \to 0$, the finite part is

$$\begin{aligned} V_f(s) &= \lim_{w\to 0} V_3[P_s;s] = \int_4^\infty \frac{\beta d\sigma}{\sigma} v(s,\sigma)\,,\\ v(s,\sigma) &= \frac{1}{(16\pi^2)^2} \int_0^1 (1 + s x_2(1 - 3x_2))dx_2\\ &\quad \times \int_0^1 \frac{x_3^3 dx_3}{z_3}\,. \end{aligned} \tag{24}$$

For $\gamma\gamma \to \pi\pi$, this representation is not well suited, because V_f contains a branch point at $s = 4$, and the physical region for $\gamma\gamma \to \pi\pi$ is $s \geq 4$. This branch point manifests itself in a zero in the denominator of the integrand in (24) along the curve $z_3 = 0$ in the square $0 \leq x_2, x_3 \leq 1$. One may solve the problem by writing a dispersion relation for V_f. Using

$$\frac{1}{z_3} = P(\frac{1}{z_3}) + i\pi\delta(z_3) \tag{25}$$

for $s \to s + i0^+$, we obtain

$$\begin{aligned} \mathrm{Im}v(s,\sigma) &= \frac{\pi}{(16\pi^2)^2} \int_{x_{2_-}}^{x_{2_+}} dx_2 x_{3_+}^3 \frac{1 + s x_2(1 - 3x_2)}{W_\sigma}\,,\\ &\quad s > 4\,,\\ x_{2_\pm} &= \frac{1}{2}(1 \pm (1 - 4/s)^{1/2})\,,\\ x_{3_+} &= \frac{1}{2y_2}(\sigma - W_\sigma)\,,\ W_\sigma = (\sigma^2 - 4\sigma y_2)^{1/2}\,, \end{aligned} \tag{26}$$

from where

$$v(s,\sigma) = \frac{1}{\pi}\int_4^\infty \frac{dz}{z-s}\mathrm{Im}v(z,\sigma)\,.$$

Integration over σ gives

$$V_f(s) = \frac{1}{\pi}\int_4^\infty \frac{dz}{z-s}\int_4^\infty \frac{d\sigma}{\sigma}\,\beta\,\mathrm{Im}v(z,\sigma)\,. \qquad (27)$$

The function V_f may be expressed in terms of elementary functions [16,7],

$$V_f(s) = \frac{1}{(16\pi^2)^2}\left[\left(3-\frac{\pi^2}{3s\rho^2}\right)f + \frac{1}{2\rho^2}f^2 - \frac{1}{3s\rho^4}f^3 + \frac{25}{4} + \frac{\pi^2}{6}\right]\ , \qquad (28)$$

with

$$f = \rho\left\{\ln\frac{1-\rho}{1+\rho} + i\pi\right\}\ \ ;\ \ \rho = \sqrt{1-4/s}\ \ ,\ \ s>4\ . \qquad (29)$$

Corresponding expressions hold for any $V_3[P;s]$. In the evaluation of the matrix element for e.g. the process $\gamma\gamma \to \pi\pi$, V_3 also occurs in the box diagrams considered below. Due to the algebraic complexity of the expressions encountered, it may be more useful to use representations analogous to (27). They allow for an efficient algebraic treatment. The triple integrals required are in any case considerably easier to evaluate than the four–dimensional ones used in the box diagrams discussed below.

5 The box

We consider integrals of the type

$$\left\langle\left\langle l_1^{\mu_1}\dots l_1^{\mu_N}\prod_{i=1}^5\frac{1}{D_i}\right\rangle\right\rangle\,, \qquad (30)$$

with

$$\begin{aligned} &D_1 = 1-l_1^2\,,\ D_2 = 1-(l_1+q_1)^2\,,\\ &D_3 = 1-(l_1-q_2)^2\,,\\ &D_4 = 1-l_2^2\,,\ D_5 = 1-(l_2+l_1+q_1-p_1)^2\,. \end{aligned} \qquad (31)$$

These are generated by the diagram Fig. 4. We consider the case

$$q_1+q_2 = p_1+p_2\,,\ p_1^2=p_2^2=1\,,\ q_1^2=q_2^2=0\,,$$

that is relevant for the process $\gamma\gamma \to \pi\pi$. Similarly to the vertex diagram considered in the previous section, integration over l_2 leads us to consider the tensors

$$\begin{aligned} B^{\mu_1\dots\mu_N} &= \int_4^\infty \frac{[d\sigma]}{\sigma}\langle l_1^{\mu_1}\dots l_1^{\mu_N}\frac{\bar t}{\sigma-\bar t}\prod_{i=1}^3\frac{1}{D_i}\rangle\,,\\ \bar t &= (p_1-q_1-l_1)^2\,, \end{aligned} \qquad (32)$$

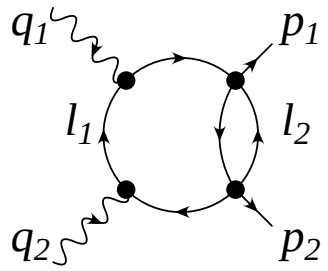

Fig. 4. The box diagram. The filled circles denote vertices from the effective lagrangian $\mathcal{L}_2$ in (2). The wavy lines stand for the electromagnetic current. The internal lines stand for scalar propagators with mass 1

where we again have dropped the nonlocal singularity generated by $J(0)$. The parametrization $\mathcal{F}[D_2D_1D_3(\sigma-\bar t)]$ gives

$$B^{\mu_1\dots\mu_N} = \int_4^\infty \frac{[d\sigma]}{\sigma}\left\{\left\langle l_1^{\mu_1}\dots l_1^{\mu_N}\frac{\bar t}{[z_4-(l_1+\delta)^2]^4}\right\rangle\right\}_{123}\,, \qquad (33)$$

with

$$\begin{aligned} z_4 &= B - Ax_1\,,\\ A &= x_2x_3\{s(1-x_2)x_3 + (1-t)(1-x_3)\} \equiv x_2x_3\bar A\,,\\ B &= A+z_3 = x_3^2 + x_2x_3(1-x_3)(1-t) + \sigma(1-x_3)\,,\\ \delta &= q_1x_1x_2x_3 - q_2x_3(1-x_2) + (q_1-p_1)(1-x_3)\,,\\ s &= (p_1+p_2)^2, t = (p_1-q_1)^2\,. \end{aligned} \qquad (34)$$

The quantity z_3 has already occurred in the vertex diagram, see (19). With the shift $l_1 \to l_1-\delta$, the momentum integrations are easily done by use of (B1), and the tensors $B^{\mu_1\dots\mu_N}$ may be expressed in terms of the scalar integrals

$$B_m[P;s,t] = \int_4^\infty \frac{[d\sigma]}{\sigma}\{P(x_1,x_2,x_3)F_m[z_4]\}_{123}\,, \qquad (35)$$

where $P(x_1,x_2,x_3)$ is a polynomial in x_1,x_2,x_3, and where the arguments s,t in $B_m[P;s,t]$ denote the s,t dependence of z_4. These integrals are convergent at $w=0$ for $m \geq 3$. We reduce the divergent integrals to the case $m=3$ by use of the recursion relation

$$\begin{aligned} B_m[P;s,t] &= V_m[3x_2x_3P_1(1,x_2,x_3);s]\\ &\quad -mB_{m+1}[AP_1(x_1,x_2,x_3);s,t]\,,\\ P_1(x_1,x_2,x_3) &= \int_0^{x_1} dy\,P(y,x_2,x_3)\,. \end{aligned} \qquad (36)$$

This relation is obtained from (35) by partial integration in x_1. The vertex functions V_m have been discussed above, and it remains to determine $B_{3,4}$. In the kinematical region where $z_4 \neq 0$, these functions may be obtained from (35) via a four–dimensional integration. In the physical region for the process $\gamma\gamma \to \pi\pi$, however, z_4 vanishes on a two–dimensional surface embedded in the hypercube

$0 \le x_1, x_2, x_3 \le 1$. Analogous singularities occur in the physical region for $\gamma\pi \to \gamma\pi$. These zeros in z_4 generate branch points at $s = 4$ and at $t = 9$. We therefore use again a Cauchy representation, and consider the region $t < 9$, where it suffices to use a fixed–t representation – the region $t > 9$ might then e.g. be reached by use of a Mandelstam representation. We illustrate the procedure for

$$G(s,t) = \lim_{w\to 0} B_3[P;s,t] = \int_4^\infty \frac{d\sigma}{\sigma}\,\beta g(\sigma;s,t)\,,$$
$$g = \frac{1}{2(16\pi^2)^2}\left\{\frac{P(x_1,x_2,x_3)}{z_4}\right\}_{123}\,. \qquad (37)$$

By use of (25), with $z_3 \to z_4$, we obtain for the discontinuity of g

$$\begin{aligned}\mathrm{disc}_s g(\sigma;s,t) &\doteq g(\sigma;s+i0^+,t) - g(\sigma;s+i0^-,t)\\ &= \frac{6\pi i}{(16\pi^2)^2}\int_{x_{2-}}^{x_{2+}} dx_2 \int_{x_{3+}}^1 \frac{x_3}{\overline{A}}\\ &\quad\times P\left(\frac{B}{A},x_2,x_3\right)dx_3\,, \qquad (38)\end{aligned}$$

where $x_{2\pm}, x_{3+}$ are given in (26). Therefore,

$$G(s,t) = \frac{1}{2\pi i}\int_4^\infty \frac{dz}{z-s}\int_4^\infty \frac{d\sigma}{\sigma}\,\beta\,\mathrm{disc}_s g(\sigma;z,t)\,. \qquad (39)$$

In case that the polynomial P contains the variable s, one has to make sure to generate the correct asymptotic behaviour through the dispersive representation. It may be necessary to pull out factors of s in the numerator before doing the dispersive integral – it is in any case useful to check the dispersive representation in a region free of cuts by use of (35). Analogous expressions can be obtained for B_4, e.g. by first integrating over x_1 and then again using (25).

6 The acnode

We consider the tensorial integral

$$A^{\mu\nu} = \left\langle\left\langle\, l_1^\mu l_2^\nu \prod_{i=1}^5 \frac{1}{D_i}\right\rangle\right\rangle\,, \qquad (40)$$

that is generated by the acnode diagram Fig. 5, with

$$\begin{aligned}&D_1 = 1-l_1^2\,,\ D_2 = 1-(l_1+q_1)^2\,,\ D_3 = 1-l_2^2\,,\\ &D_4 = 1-(l_2+q_2)^2\,,\ D_5 = 1-(l_2-l_1+p_1-q_1)^2\,,\\ &q_1+q_2 = p_1+p_2\,,\\ &q_1^2 = q_2^2 = 0,\ \ p_1^2 = p_2^2 = 1\,. \qquad (41)\end{aligned}$$

The first step in the calculation [17] is to employ the Feynman parametrization as $\mathcal{F}[D_1D_2]\,\mathcal{F}[D_4D_3]$ such that

$$\begin{aligned}A^{\mu\nu} &= \int_0^1 dx_1\int_0^1 dx_2\\ &\quad\times\left\langle\left\langle\frac{(l_1-(1-x_1)q_1)^\mu (l_2-x_2q_2)^\nu}{(1-l_1^2)^2(1-l_2^2)^2(1-(l_1-l_2+k)^2)}\right\rangle\right\rangle\,,\\ k &= x_1q_1+x_2q_2-p_1\,. \qquad (42)\end{aligned}$$

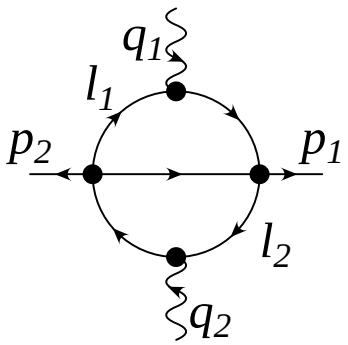

Fig. 5. The acnode diagram. The filled circles denote vertices from the effective lagrangian $\mathcal{L}_2$ in (2). The wavy lines stand for the electromagnetic current. The internal lines stand for scalar propagators with mass 1

The integrals d^dl_1 can now be performed once the denominators $(1-l_1^2)^2$ and $(1-(l_1-l_2+k)^2)$ are combined. The result is proportional to

$$\int_0^1 dx_3\,x_3\,\frac{[(1-x_3)(l_2-k)^\mu-(1-x_1)\,q_1^\mu]}{[1-x_3(1-x_3)(l_2-k)^2]^{1-w}}.$$

The integrals d^dl_2 can be done by combining

$$(1-l_2^2)^2([x_3(1-x_3)]^{-1}-(l_2-k)^2)^{1-w}$$

in the standard manner. The expression $A^{\mu\nu}$ then consists of a convergent part proportional to tensors built from the external momenta, and a divergent piece proportional to $g^{\mu\nu}$. The convergent part is easy to evaluate numerically in the physical region for $\gamma\gamma \to \pi\pi$, because it does not contain branch points there. In case one wishes to evaluate these terms e.g. at $(q_1-p_1)^2 \ge 9$, one may again write a dispersion relation for the form factors in question. Here, we concentrate on the term proportional to $g^{\mu\nu}$,

$$\begin{aligned}A^{\mu\nu} &= A_0 g^{\mu\nu} + \cdots\,,\\ A_0 &= -C^2(w)\Gamma(-2w)\frac{1}{2}\int_0^1 d^4x[x_3(1-x_3)]^{-w}\\ &\quad\times x_4(1-x_4)^{-w}\,{z_5}^{2w}\,,\end{aligned} \qquad (43)$$

where

$$z_5 = 1-x_4+x_3(1-x_3)x_4\left\{1-(1-x_4)k^2\right\}\,. \qquad (44)$$

Expanding the integrand in powers of w, we find

$$\begin{aligned}A_0 &= C(w)^2\Gamma(-w)^2\frac{w}{16}(2+7w)\\ &\quad+\frac{1}{2(16\pi^2)^2}\int_0^1 d^4x\;x_4\ln z_5 + O(w)\,. \qquad (45)\end{aligned}$$

7 Summary and conclusions

1. We have discussed in this article the two–loop diagrams that occur in the evaluation of the amplitudes

$\gamma\gamma \to \pi^0\pi^0$ in the equal mass case. These are the self–energy, the vertex, the box and the acnode graphs, displayed in Figs. 2–5. These are also all the two–loop graphs occurring in the processes listed in (1).

2. We first discuss our results for the *self–energy*, the *vertex* and the *box graphs*. These diagrams contain, as a subgraph, the one–loop function[2]

$$J(t) = \left\langle \frac{1}{(1-l_1^2)} \frac{1}{(1-(l_1-p)^2} \right\rangle \; ; \; t = p^2 \, ,$$

that we represent in a dispersive manner,

$$J(t) = \int_4^\infty \frac{[d\sigma]}{\sigma - t} \, .$$

As a result, they may be represented in d dimensions as linear combinations of the following integrals:

$$\Gamma(-w-n) \int_4^\infty [d\sigma] \{P_1 z_2^{w+n}\}_1 \text{ Fig. 2 (self–energy)}$$

$$\Gamma(-w-n) \int_4^\infty \frac{[d\sigma]}{\sigma} \left\{P_2 z_3^{w+n}\right\}_{23} \text{ Fig. 3 (vertex)}$$

$$\Gamma(-w-n) \int_4^\infty \frac{[d\sigma]}{\sigma} \left\{P_3 z_4^{w+n}\right\}_{123} \text{ Fig. 4 (box)}$$

Here, n denotes an integer, and P_k are polynomials in k Feynman parameters. The z_i are polynomials in the external momenta, in the Feynman parameters and in σ.

3. The vertex and box integrals receive further contributions, that contain a nonlocal singularity which is generated by a divergent subdiagram. These contributions are cancelled by the standard renormalization procedure, and we have not considered them further here.
4. In order to recover the finite and infinite parts in the vertex and in the box diagrams at $w \to 0$, we have performed partial integrations in the Feynman parameters, reducing in this manner the exponent in z_i^{w+n}. The finite parts are obtained by reducing the exponent to $n = -1$, while the surface terms generated by partial integration produce the divergences. In the case of the self–energy diagram, one does not obtain a finite result in this manner. We have instead subtracted the first two terms of the Taylor series expansion of z_2^w around $s = 1$.
5. In this manner, we are able to express all divergences in terms of the integrals

$$\{D(m,n) \; ; \; E(m,n)\} = \int_4^\infty [d\sigma] \left\{1 \; ; \; \frac{1}{\sigma}\right\} \times \{(1-x)^m F_n[y]\}_1 \, ,$$

where

$$y = x^2 + \sigma(1-x) \; ; \; m = 0, 1, 2 \ldots ; \;\; n = 1, 2, 3 \ldots$$

We evaluate and tabulate these quantities in appendix C.

6. In the physical region for $\gamma\gamma \to \pi^0\pi^0$, the vertex and box diagram develop branch points and cuts, as a result of which the above representation for the finite part is not appropriate. We instead write fixed–t dispersion relations. We provide an integral representation for the required absorptive part in each case.
7. The vertex diagrams can be given in closed form [16, 7]. The algebraic complexities in the case of $\gamma\gamma \to \pi\pi$ suggest, however, that it may sometimes be simpler to keep them in the form of the integral representations provided here. Needless to say that this decision is a matter of taste.
8. Finally, we come to the *acnode diagram*, shown in Fig. 5. Instead of presenting the originally used [2,5] method, we evaluate it here along lines that are similar to the ones suggested in [17] for the decay $\eta \to \pi^0\gamma\gamma$. The kinematics in $\gamma\gamma \to \pi^0\pi^0$ allows for a substantially simpler procedure than the one needed in [17].
9. We conclude that, with these methods at hand, one is able to calculate many processes at two–loop order in the framework of chiral perturbation theory.

Acknowledgements. We thank S. Bellucci, J. Bijnens, U. Bürgi, G. Colangelo, G. Ecker and P. Talavera for enjoyable discussions and collaboration at various stages of this work. In particular, we thank J. Bijnens, G. Colangelo and P. Talavera for checking our result for the self–energy and for the vertex diagrams, and for useful comments on the manuscript. One of us (JG) has been partially supported by the Swiss National Science Foundation. He furthermore acknowledges the warm hospitality of the University of Granada, where this work was completed. The other author (MES) thanks Oskar Öflunds Stiftelse for a travel grant.

Appendix

A Notation

To simplify the notation, we set the pion masses equal to one,

$$M_{\pi^\pm} = M_{\pi^0} = 1 \, .$$

As is customary, we use dimensional regularization and put

$$w = \frac{d}{2} - 2 \, ,$$

where d denotes the dimension of space-time. Loop integrations are symbolized by a bracket,

$$\langle \ldots \rangle = \int \frac{d^d l_1}{i(2\pi)^d} (\ldots) \, ,$$
$$\langle\langle \ldots \rangle\rangle = \int \frac{d^d l_1}{i(2\pi)^d} \int \frac{d^d l_2}{i(2\pi)^d} (\ldots) \, . \qquad \text{(A1)}$$

We combine denominators with

$$[a_1 \ldots a_N]^{-1} = \int [dx]_{N-1} [a_1 x_1 \ldots x_{N-1}$$

[2] For the notation, see appendix A

$$
\begin{aligned}
&+a_2x_2\dots x_{N-1}(1-x_1)\\
&+a_3x_3\dots x_{N-1}(1-x_2)\\
&\vdots\\
&+a_N(1-x_{N-1})]^{-N}\\
&\equiv \mathcal{F}[a_1\dots a_N]. \qquad \text{(A2)}
\end{aligned}
$$

Here $[dx]_N$ stands for the normalized measure

$$
\begin{aligned}
[dx]_N &= N!\prod_{\nu=1}^{N}\theta[x_\nu(1-x_\nu)]x_\nu^{\nu-1}dx_\nu\,,\\
\int[dx]_N &= 1\,, \qquad \text{(A3)}
\end{aligned}
$$

and $\theta(x)$ denotes the step function. We abbreviate multiple Feynman integrals by

$$
\begin{aligned}
\{\dots\}_1 &= \int_0^1 dx\{\dots\}\,,\\
\{\dots\}_{23} &= 2\int_0^1 dx_2\int_0^1 x_3dx_3\{\dots\}\,,\\
\{\dots\}_{123} &= 6\int_0^1 dx_1\int_0^1 x_2dx_2\int_0^1 x_3^2dx_3\{\dots\}\,. \qquad \text{(A4)}
\end{aligned}
$$

Furthermore, we use the measure

$$
[d\sigma] = \frac{C(w)\Gamma(3/2)}{\Gamma(3/2+w)}(\frac{\sigma}{4}-1)^w\beta\; d\sigma\,, \qquad \text{(A5)}
$$

with

$$
C(w) = \frac{1}{(4\pi)^{2+w}}\,, \quad \beta = (1-4/\sigma)^{1/2}\,, \qquad \text{(A6)}
$$

and

$$
\lim_{w\to 0}[d\sigma] = \frac{\beta}{16\pi^2}\; d\sigma\,. \qquad \text{(A7)}
$$

B One–loop integrals

In the text we use the loop–functions

$$
\begin{aligned}
\left\langle\frac{1}{[z-l_1^2]^m}\right\rangle &= F_m[z]\,,\\
\left\langle\frac{l_1^\mu l_1^\nu}{[z-l_1^2]^m}\right\rangle &= -\frac{g^{\mu\nu}}{2(m-1)}\;F_{m-1}[z]\,,\\
\left\langle\frac{l_1^\mu l_1^\nu l_1^\rho l_1^\sigma}{[z-l_1^2]^m}\right\rangle &= \frac{g^{\mu\nu}g^{\rho\sigma}+\text{cycl.}}{4(m-1)(m-2)}\;F_{m-2}[z]\,. \qquad \text{(B1)}
\end{aligned}
$$

They are given by

$$
F_m[z] = z^{w+2-m}C(w)\frac{\Gamma(m-2-w)}{\Gamma(m)}\,,\; m\geq 1\,. \qquad \text{(B2)}
$$

In particular,

$$
\begin{aligned}
&(F_1\,;\,F_2\,;\,F_3\,;\,F_4) = z^w\,C(w)\\
&\times\left(\Gamma(-1-w)z\,;\,\Gamma(-w)\,;\,\frac{\Gamma(1-w)}{2z}\,;\,\frac{\Gamma(2-w)}{6z^2}\right). \qquad \text{(B3)}
\end{aligned}
$$

We also use

$$
J(t) = \left\langle\frac{1}{1-l_1^2}\frac{1}{1-(l_1-p)^2}\right\rangle\,;\; t=p^2\,, \qquad \text{(B4)}
$$

with

$$
J(0) = C(w)\Gamma(-w)\,. \qquad \text{(B5)}
$$

C The integrals $D(m,n)$ and $E(m,n)$

Here we consider the integrals

$$
\begin{aligned}
\{D(m,n)\,;\;E(m,n)\} &= \int_4^\infty[d\sigma]\left\{1\,;\;\frac{1}{\sigma}\right\}\\
&\times\int_0^1 dx\,(1-x)^m F_n[y] \qquad \text{(C1)}
\end{aligned}
$$

where

$$
y = x^2+\sigma(1-x)\,;\; m=0,1,2\dots\,,\; n=1,2,3\dots
$$

In particular, we determine the divergent parts in $D(m,n\leq 3)$ and in $E(m,n\leq 2)$. By partial integration in x, we obtain the recursion relation

$$
\begin{aligned}
(3+w+m-n)D(m,n) &= \frac{\Gamma(n-w-2)Q(w+2-n)}{\Gamma(n)\Gamma(-w)}\\
&-n\left\{D(m,n+1)-D(m+2,n+1)\right\}\,, \qquad \text{(C2)}
\end{aligned}
$$

with

$$
\begin{aligned}
Q(\alpha) &= C(w)\Gamma(-w)\int_4^\infty[d\sigma]\;\sigma^\alpha\\
&= C^2(w)\Gamma(-w)\Gamma(-1-w-\alpha)\frac{\Gamma(-\alpha)}{\Gamma(-2\alpha)}\,. \qquad \text{(C3)}
\end{aligned}
$$

An analogous relation holds for $E(m,n)$, with $Q(w+2-n)\to Q(w+1-n)$. One may use these recursion relations to express $D(m\geq 1,n\leq 3)$ and $E(m,n\leq 2)$ through the divergent quantities Q and the convergent integrals $D(m\geq 1,4)$ and $E(m,3)$. The case $D(0,n)$ must be treated separately, see below.

C.1 Explicit expressions for $D(m,n)$

Let

$$
\begin{aligned}
D(m,n) &= C^2(w)\Gamma^2(-w)\left\{p(m,n,0)+wp(m,n,1)\right.\\
&\left.+w^2p(m,n,2)+O(w^3)\right\}\,. \qquad \text{(C4)}
\end{aligned}
$$

For $m\geq 1$, we proceed as described above and find

$$
\begin{aligned}
p(m,1,0) &= (m^2+4m+5)m(m+4)N_4,\\
p(m,1,1) &= -(2m^7+29m^6+172m^5+540m^4+964m^3\\
&\quad +951m^2+430m+36)m(m+4)N_4^2,\\
p(m,1,2) &= \{m(m+1)D(m+6)-3m(m+3)D(m+4)\\
&\quad +3(m+1)(m+4)D(m+2)
\end{aligned}
$$

$$
\begin{aligned}
&-(m+3)(m+4)D(m)\}\,N_4\\
&+\big(3m^{12}+74m^{11}+812m^{10}+5230m^9\\
&+21938m^8+62724m^7+123986m^6\\
&+167682m^5+149409m^4+81146m^3\\
&+23372m^2+3456m+864\big)\,m(m+4)N_4^3,\\
p(m,2,0) &= -m(m+2)N_2,\\
p(m,2,1) &= (2m^3+7m^2+7m+1)m(m+2)N_2^2,\\
p(m,2,2) &= \{mD(m+4)-2(m+1)D(m+2)\\
&+(m+2)D(m)\}\,N_2\\
&-\big(4m^6+26m^5+61m^4+63m^3+27m^2\\
&+4m+2\big)\,m(m+2)N_2^3\\
p(m,3,0) &= 0,\\
p(m,3,1) &= -1/(4m),\\
p(m,3,2) &= \{D(m+2)-D(m)\}/(2m)\\
&-(2m-1)/(4m^2),
\end{aligned}
\tag{C5}
$$

where

$$
\begin{aligned}
&N_2^{-1}=m(m+1)(m+2),\ N_4^{-1}=N_2^{-1}(m+3)(m+4),\\
&D(m)=\int_4^\infty d\sigma\beta\int_0^1\frac{dx(1-x)^m}{\{x^2+\sigma(1-x)\}^2}\\
&\quad=\int_0^1 dx\frac{x^{m-1}}{(1-x)^2}\left(1+\frac{2x}{1-x^2}\ln x\right).
\end{aligned}
\tag{C6}
$$

For example,

$$
\begin{aligned}
&D(1)=(\pi^2-4)/16,\ D(2)=-(\pi^2-12)/16,\\
&D(3)=-(13\pi^2-132)/48\,.
\end{aligned}
\tag{C7}
$$

In Table 1, we display some of the coefficients $p(m,n,k)$ for convenience. We now turn to $D(0,n)$ which is divergent for any n. The recursion relation (C2) allows one to evaluate $D(0,1)$ and $D(0,3)$ from

$$
\begin{aligned}
D(0,2) &= C(w)\Gamma(-w)\int_4^\infty[d\sigma]\\
&\times\int_0^1 dx\,\left(x^2+\sigma(1-x)\right)^w,
\end{aligned}
\tag{C8}
$$

and from $D(m\geq 2,n)$. In order to evaluate $D(0,2)$, we add and subtract from the integrand in (C8) the quantity

$$
\triangle=(x+\sigma(1-x))^w-\frac{wx}{\sigma}\left(\sigma(1-x)\right)^w.
$$

The integral

$$
C(w)\Gamma(-w)\int_4^\infty[d\sigma]\int_0^1 dx\,\left((x^2+\sigma(1-x))^w-\triangle\right)
\tag{C9}
$$

is finite at $w=0$, whereas the divergence is contained in

$$
C(w)\Gamma(-w)\int_4^\infty[d\sigma]\int_0^1 dx\,\triangle\,.
\tag{C10}
$$

In this manner, we obtain the values $p(0,n\leq 3,k)$ displayed in Table 1.

Table 1. The coefficients $p(m,n,k)$

m	n	$p(m,n,0)$	$p(m,n,1)$	$p(m,n,2)$
0	1	$\frac{13}{12}$	$-\frac{469}{144}$	$\frac{10445}{1728}$
1	1	$\frac{5}{12}$	$-\frac{781}{720}$	$\frac{78121}{43200}$
2	1	$\frac{17}{60}$	$-\frac{2389}{3600}$	$\frac{233857}{216000}$
0	2	$-\frac{3}{2}$	$\frac{17}{4}$	$-\frac{59}{8}$
1	2	$-\frac{1}{2}$	$\frac{17}{12}$	$-\frac{59}{24}$
2	2	$-\frac{1}{3}$	$\frac{59}{72}$	$-\frac{1333}{864}$
0	3	$\frac{1}{4}$	$-\frac{1}{2}$	$-\frac{\pi^2}{6}+1$
1	3	0	$-\frac{1}{4}$	$-\frac{\pi^2}{6}+\frac{5}{4}$
2	3	0	$-\frac{1}{8}$	$-\frac{\pi^2}{6}+\frac{23}{16}$
3	3	0	$-\frac{1}{12}$	$-\frac{\pi^2}{6}+\frac{3}{2}$
4	3	0	$-\frac{1}{16}$	$-\frac{\pi^2}{6}+\frac{883}{576}$

C.2 Explicit expressions for $E(m,n)$

Let

$$
\begin{aligned}
E(m,n) &= C^2(w)\Gamma^2(-w)\,\{q(m,n,0)+wq(m,n,1)\\
&+w^2q(m,n,2)+O(w^3)\}\,.
\end{aligned}
\tag{C11}
$$

Proceeding in the manner described above, we find

$$
\begin{aligned}
q(m,1,0) &= (m^2+4m+2)N_3,\\
q(m,1,1) &= -(3m^5+31m^4+124m^3+235m^2+205m\\
&+64)N_3^2,\\
q(m,1,2) &= \{(m+1)E(m+4)-2(m+2)E(m+2)\\
&+(m+3)E(m)\}\,N_3+\big(7m^8+115m^7\\
&+802m^6+3097m^5+7230m^4\\
&+10425m^3+9041m^2+4295m+848\big)\,N_3^3,\\
q(m,2,0) &= N_1/2,\\
q(m,2,1) &= (2m+1)N_1^2/2,\\
q(m,2,2) &= \{E(m+2)-E(m)\}\,N_1\\
&+(4m^2+6m+3)N_1^3/2,
\end{aligned}
\tag{C12}
$$

where

$$
\begin{aligned}
&N_1^{-1}=(m+1),\ N_3^{-1}=N_1^{-1}(m+2)(m+3),\\
&E(m)=\int_4^\infty\frac{d\sigma}{\sigma}\beta\int_0^1\frac{dx(1-x)^m}{x^2+\sigma(1-x)}\\
&\quad=-\int_0^1 dx\frac{x^m}{(1-x)^2}\left(2+\frac{1+x}{1-x}\ln x\right).
\end{aligned}
\tag{C13}
$$

Table 2. The coefficients $q(m,n,k)$

m	n	$q(m,n,0)$	$q(m,n,1)$	$q(m,n,2)$
0	1	$\frac{1}{3}$	$-\frac{16}{9}$	$\frac{223}{54}$
1	1	$\frac{7}{24}$	$-\frac{331}{288}$	$\frac{9011}{3456}$
2	1	$\frac{7}{30}$	$-\frac{1499}{1800}$	$\frac{206087}{108000}$
0	2	$\frac{1}{2}$	$\frac{1}{2}$	$\frac{2\pi^2}{3}-\frac{11}{2}$
1	2	$\frac{1}{4}$	$\frac{3}{8}$	$\frac{2\pi^2}{3}-\frac{93}{16}$
2	2	$\frac{1}{6}$	$\frac{5}{18}$	$\frac{2\pi^2}{3}-\frac{325}{54}$
3	2	$\frac{1}{8}$	$\frac{7}{32}$	$\frac{2\pi^2}{3}-\frac{7073}{1152}$
4	2	$\frac{1}{10}$	$\frac{9}{50}$	$\frac{2\pi^2}{3}-\frac{27983}{4500}$

For example

$$E(0)=\frac{1}{2},\ E(1)=\frac{\pi^2-9}{6},\ E(2)=\frac{4\pi^2-39}{6}\,. \quad \text{(C14)}$$

For convenience, we display some of the coefficients $q(m,n,k)$ in Table 2.

References

1. S. Weinberg: Physica 96A (1979) 327; J. Gasser and H. Leutwyler: Ann. Phys. (N.Y.) 158 (1984) 142; Nucl. Phys. B250 (1985) 465
2. S. Bellucci, J. Gasser and M.E. Sainio: Nucl. Phys. B423 (1994) 80; ibid. B431 (1994) 413 (E)
3. J. Bijnens and F. Cornet: Nucl. Phys. B296 (1988) 557; J.F. Donoghue, B.R. Holstein and Y.C. Lin: Phys. Rev. D37 (1988) 2423
4. Crystal Ball Collab., H. Marsiske et al.: Phys. Rev. D41 (1990) 3324
5. U. Bürgi: PhD thesis, University of Berne, 1996; Phys. Lett. B377 (1996) 147; Nucl. Phys. B479 (1996) 392
6. J. Bijnens and P. Talavera: Nucl. Phys. B489 (1997) 387
7. J. Bijnens et al.: Phys. Lett. B374 (1996) 210; Nucl. Phys. B508 (1997) 263
8. E. Golowich and J. Kambor: Nucl. Phys. B447 (1995) 373; Phys. Rev. D53 (1996) 2651
9. E. Golowich and J. Kambor: Phys. Rev. **D58** (1998) 036004; Phys. Rev. Lett. 79 (1997) 4092
10. P. Post and K. Schilcher: Phys. Rev. Lett. 79 (1997) 4088
11. J. Bijnens: *Goldstone Boson Production and Decay*, in: Proceedings of the Chiral Dynamics Workshop, Sept. 1–5, 1997, Mainz, Germany, to appear, hep–ph/9710341
12. J. Bijnens, G. Colangelo and P. Talavera: hep-ph/9805389; J. High Energy Phys. **05** (1998) 014
13. P. Post and J.B. Tausk: Mod. Phys. Lett. A11 (1996) 2115
14. P.N. Maher, L. Durand and K. Riesselmann: Phys. Rev. D48 (1993) 1061; ibid. D52 (1995) 553 (E)
15. We have been inspired to this approach by the work of G. Barton and C. Kacser: Nuovo Cim. 21 (1961) 593; J.B. Bronzan and C. Kacser: Phys. Rev. 132 (1963) 2703
16. D. Bessis and M. Pusterla: Nuovo Cim. A54 (1968) 243
17. M. Jetter: Nucl. Phys. B459 (1996) 283